CrystEngComm

Accepted Manuscript

ROYAL SOCIETY OF CHEMISTRY

www.rsc.org/crystengcomm

Macroscopic Glass-Permeated Single-Crystals of Fresnoite

Wolfgang Wisniewski, Marcus Nagel, Christian Rüssel

Otto-Schott-Institut, Jena University, Fraunhoferstr. 6, 07743 Jena, Germany

Summary

Macroscopic glass-permeated single-crystals of fresnoite ($Ba_2TiSi_2O_8$, BTS) are grown by a Czochralski-like procedure initiated by electrochemically induced nucleation (EiN). Morphological and crystallographic properties of these materials are analyzed using scanning electron microscopy (SEM) and electron backscatter diffraction (EBSD) before and after annealing at 1150 °C for 23 h. While continuous orientation changes of 8 °/mm are observed in dendritic single crystals competing with others during growth, only changes of 0.2 °/mm are observed in a freely grown dendrite over an area of more than 1 cm^2. A type of intragranular Ostwald ripening and the formation of the high temperature phase of $BaSi_2O_5$ occur during annealing. Two phase separated residual glasses are observed between the crystals.

Corresponding author: Wolfgang Wisniewski
Fraunhoferstr. 6, 07743 Jena
Otto-Schott-Institut, Jena University
Tel: (0049) 03641 948515
Fax: (0049) 03641 948502
wolfgang.w@uni-jena.de

Macroscopic Glass-Permeated Single-Crystals of Fresnoite

Wolfgang Wisniewski, Marcus Nagel, Christian Rüssel

Otto-Schott-Institut, Jena University, Fraunhoferstr. 6, 07743 Jena, Germany

Summary

Macroscopic glass-permeated single-crystals of fresnoite ($Ba_2TiSi_2O_8$, BTS) are grown by a Czochralski-like procedure initiated by electrochemically induced nucleation (EiN). Morphological and crystallographic properties of these materials are analyzed using scanning electron microscopy (SEM) and electron backscatter diffraction (EBSD) before and after annealing at 1150 °C for 23 h. While continuous orientation changes of 8 °/mm are observed in dendritic single crystals competing with others during growth, only changes of 0.2 °/mm are observed in a freely grown dendrite over an area of more than 1 cm^2. A type of intragranular Ostwald ripening and the formation of the high temperature phase of $BaSi_2O_5$ occur during annealing. Two phase separated residual glasses are observed between the crystals.

1. Introduction

Macroscopic crystal bodies of aligned orientation are widely used to access the specific properties of crystalline phases. While single crystals are the obvious option for these applications, they are usually quite expensive to produce and sometimes show unfavourable mechanical properties such as a high cleavability. An alternative option to produce crystallographically aligned materials is localized nucleation followed by growth selection, e.g. the surface crystallization of glasses. This usually only enables to produce materials with a fiber texture where e.g. one crystallographic direction is aligned but the rotation around it is random. A third option is the large scale dendritic

growth in glasses which can lead to a glass/crystal composite with only one crystal orientation. A negligible nucleation rate in the matrix and a high growth velocity are prerequisites for achieving crystal bodies in the macroscopic scale. Such dendrites have e.g. been grown by crystallizing yttrium aluminium garnet (YAG) from glass in a classic annealing procedure[1] but mainly by growing fresnoite from a glass melt using electrochemically induced nucleation (EiN)[2-7] which was first reported in 1996.[2]

EiN is a method where nucleation is limited to a chemically modified zone around a cathode in the glass melt. The experimental setup is outlined in Ref. 8 in detail. It is a nearly universally applicable technique and has been applied to produce samples containing oriented Ba/Sr-fresnoite ($Ba/Sr_2TiSi_2O_8$)[2-8] but also mullite,[9] diopside,[10] $Li_2Si_2O_5$[11] and $LiNbO_3$[12] glass-ceramics. Materials containing oriented fresnoite are of interest due to the piezoelectric,[13] pyroelectric,[13] surface acoustic[14] and non linear optical[15] properties of the crystal. As fresnoite is a non-ferroelectric polar phase, these materials cannot be poled but must be oriented during growth to access these properties. Because the polarity originates from the unit cell, these materials do not show a Curie-Temperature above which they lose their piezoelectric properties and are hence of special interest for high temperature applications.

EiN of a $Ba_2TiSi_2O_8$ (BTS) melt leads to some corrosion of the Pt-cathode[4] and the formation of a monoclinic high temperature phase with the composition $BaSi_2O_5$ (ICSD 10-0314) in a radius of ca. 300 µm around the cathode.[5] After the melt is heated above the liquidus temperature T_L to eliminate any crystalline components, it is cooled to a temperature below T_L but too high for spontaneous nucleation. While there is a thermodynamic driving force towards crystallization at this temperature, the melt cannot crystallize for kinetic reasons as nuclei are not formed. Nucleation is then triggered by electrochemically reducing Ti^{4+} to Ti^{3+} in the melt which

increases the nucleation rate due to a decrease of the melt viscosity.[8] The resulting crystals proceed to grow into the unreduced melt. Ti^{3+} was detected at a distance of ca. 2 mm from the cathode[16] in a static setup. As there is no nucleation outside of the reduced zone, these crystals are only hindered by their neighbors during growth.

In this article, we apply a Czochralski-like procedure which enabled to draw a glass-permeated single-crystal more than 10 cm long and more than 1 cm^2 surface area at the tip. We also present results characterizing the dendritic microstructure at different stages of growth before and after annealing a grown dendrite at 1150°C for 23 h.

2. Results and Discussion

BTS dendrites produced via EiN have been grown to form glass-permeated single-crystals up to 10 cm long and with a cross section of more than 1 cm^2 near the tip by slowly drawing the growing crystals out of the melt in a Czochralsky-like procedure. The drawing speed during the process approximately equals the crystal growth velocity. Figure 1 a) shows a sample drawn from the melt including the Pt-wire, the area of initial crystal growth along the melt surface where orientation selection occurs, and finally the single BTS dendrite which survived the growth selection.

Figure 1 b) shows two BTS dendrites for comparison which were formed without drawing the growing crystals out of the melt. These dendrites competed with each other during growth. The principal shape of a freely grown dendrite is illustrated below: the cross section is a more or less regular square which increases in diameter during the growth process. The growth front shows a central depression at the core while the perimeter grows faster and forms tips at the edges. Some of these observations were also made in freely grown YAG dendrites[1] or mullite needles[9] and

have been explained by the differences of 3-D diffusion in the glass matrix at the respective localities.

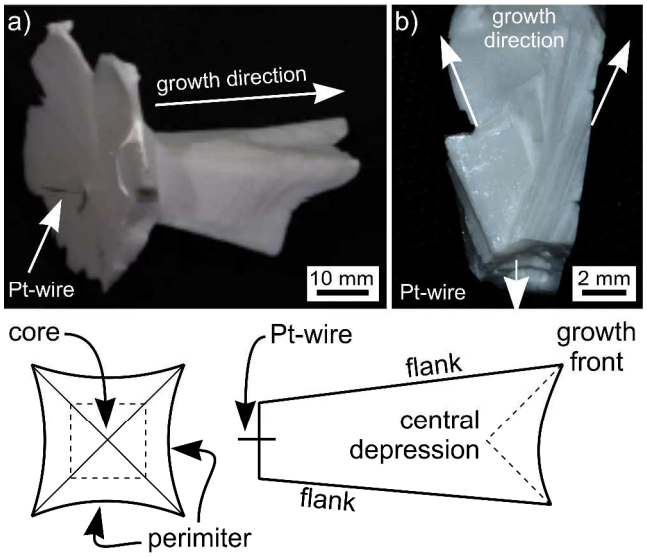

Figure 1: Images of a) a BTS single dendrite drawn from a melt and b) two BTS dendrites competing during growth away from the nucleation zone around the Pt-wire. The principal morphology is illustrated below.

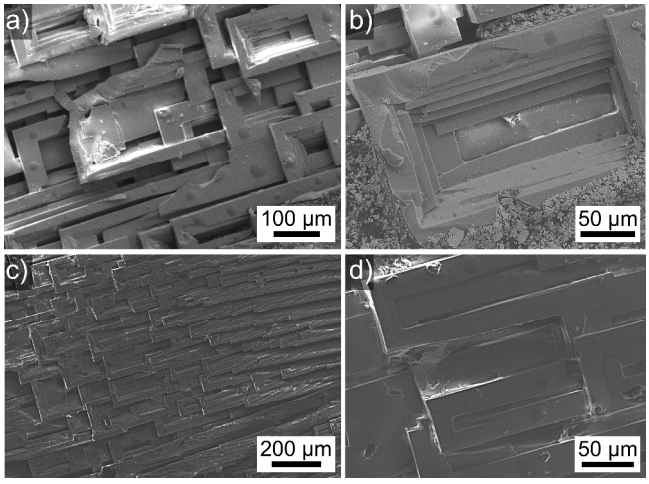

Figure 2: SEM-micrographs of fractured BTS dendrites: a) fracture plane perpendicular to the growth direction, b) the same, in greater detail. c) fracture plane parallel to the growth direction, d) the same, in greater detail.

A 3-D impression of the dendritic structures may be provided from the fracture planes perpendicular and parallel to the growth direction presented in Figure 2. They show that the dendritic branches form rectangular, spiraling funnels in the direction of the c-axis. High vacuum SEM-analysis of these structures is problematic because of charge up which is difficult to prevent due to the high surface roughness. EBSD-analysis was not possible as the carbon layer necessary to minimize charge up is too thick to enable EBSD-pattern acquisition.

SEM-micrographs featuring dendrite surfaces after pulling the latter from the melt were hence obtained using a low-vacuum SEM to avoid charge up. The Figures 3 a) and b) illustrate the morphology of the frontal growth front while Figure 3 c) features the flank of a dendrite. Figure 3 d) presents the growth structures from the flank at the edge to the frontal growth front. Based on previous measurements, it is justified to assume that basically all the structures observed in these figures share the same crystal lattice indicating they are all connected and part of the same dendrite.

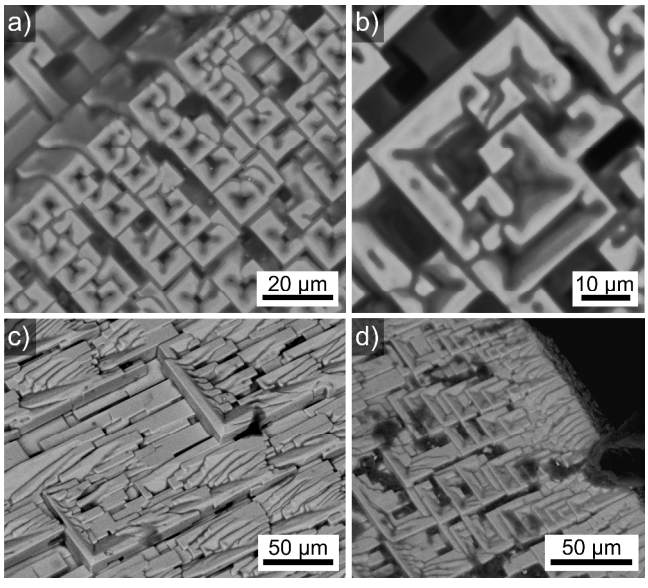

Figure 3: SEM-micrographs obtained from a) and b) the frontal growth front as well as c) and d) from the flanks of a fresnoite dendrite pulled out of the melt.

Development of a single BTS dendrite over time and distance

Figure 4 shows optical micrographs from the cross section of a glass-permeated single-crystal grown to a size of ca. 13x13 mm^2. EBSD-patterns were obtained at the locations 1-7 and the Euler Angle triplets of the evaluated orientations are presented in Table 1. As the Euler Angle Φ describes the tilt of the c-axis from the normal of the SEM-stage in this system, the value of Φ=3.7 for pattern 1 shows that the sample was mounted at a slight tilt. The patterns 2-4 all show a shift of Φ towards lower values while the patterns 5-7 show a shift towards higher values. This means that the c-axis of this dendrite slightly shifts from the central orientation by about 1.5° over a distance of ca. 7.5 mm, i.e. by 0.2°/mm. The wire frame of the orientation calculated from pattern 1 shows that the {110} planes form the flanks of the dendrite in agreement to Ref. 4. The framed area is presented in greater detail which shows that the outer parts of the dendrite show layers or steps of BTS growth around the central, rectangular core which was e.g. also observed in a large YAG dendrite.[1] Pattern 7 was obtained from this area and proves that these steps show the same orientation as the core i.e. they are part of the same dendrite. These areas are much less pronounced if dendrites compete for space during growth.[4]

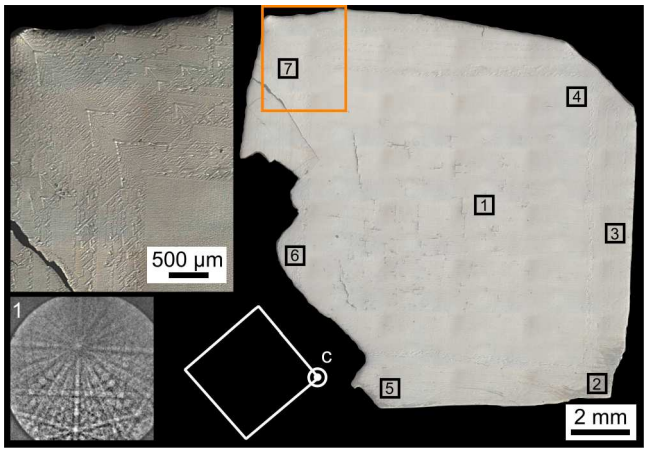

Figure 4: Optical micrograph of a single BTS dendrite cut almost perpendicular to its growth direction. The framed area is presented in greater detail (right). EBSD-patters were obtained at the locations 1-7 Pattern 1 is presented and a wire frame of the corresponding unit cell illustrates the crystal orientation evaluated from this pattern.

Table 1: Euler Angles of the orientation evaluated from the EBSD-patterns 1-7.

pattern	**φ_1**	**Φ**	**φ_2**
1 (center)	2.8	3.7	128.4
2	4.4	2.5	127.0
3	124.9	2.2	5.7
4	177.4	2.0	46.1
5	135.6	5.2	360.0
6	38.5	5.3	183.6
7	205.6	5.0	292.4

Multiple morphologies of the primary dendritic structure as well as the interdendritic areas may be observed in these materials: Figure 5 presents SEM-micrographs from cut planes perpendicular to the c-axes of such dendrites obtained a) close to the Pt-wire and b), c) after ca. 4 mm of growth. Primary dendrites not drawn from the melt are frequently surrounded by a layer of honeycomb growth followed by lamellar structures as shown in Figure 5 d) and in agreement with the literature.[3,5,6] While the primary crystals in Figure 5 a) show comparably rounded structures with few tips, the interdendritic area rather implies a phase separation than dendritic growth. The seaweed structures observed in the Figures 5 c) and d) have been linked to dendritic growth via the degree of undercooling[17] and the formation of honeycomb and lamellar structures can be explained by diffusion at these specific localities.[5] This multitude of morphologies indicates that they decisively depend on the thermal conditions between the dendrite arms and that the temperature/time schedule plays an important role after growth and especially during the cooling to room temperature.

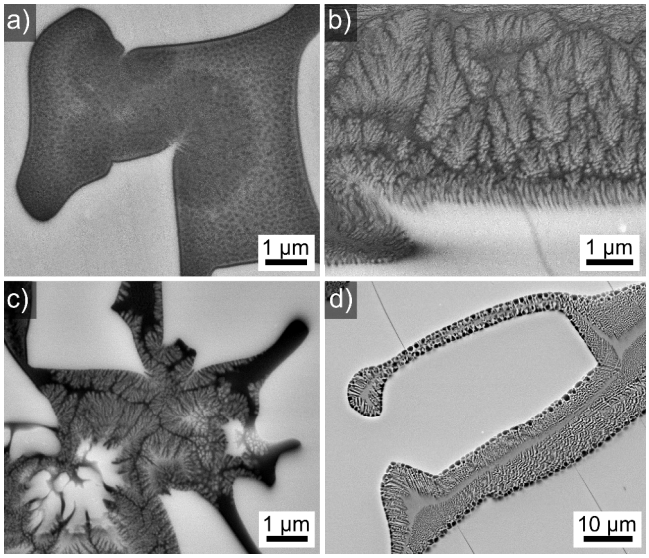

Figure 5: SEM-micrographs obtained from cross sections through fresnoite dendrites grown by EiN: a) rounded primary crystals with phase separation structures in the interdendritic space, b) Seawead structures c) Seawead structures with a tendency towards more regular dendritic growth and d) honey comb areas and lamellae.

In order to analyze the long term high temperature stability of such a glass-permeated single-crystal, the drawn dendrite already featured in the Figures 5 a) and c) was annealed at 1150 °C for 21 h, i.e. 50 °C below the growth temperature. The sample surfaces were slightly deformed as illustrated by Figure 6: generally the primary structures remain rather stable while the interdendritic areas show some swelling a). Locally the residual glass swells into mounds b) and rarely a primary crystal is also pushed upwards c), i.e. probably broken from its connection to the dendrite. As these dendrites contain some pores, the driving force for these surface modifications could be stresses due to gas bubbles beneath the surface which expand during heating.

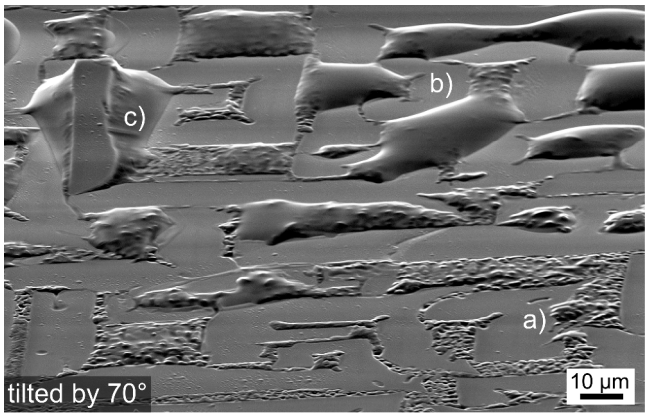

Figure 6: SEM-micrograph of an annealed surface tilted by 70°.

The samples were thus repolished in order to obtain results comparable to those obtained before annealing. Figure 7 features the microstructure near the Pt-wire a) at the core and b) at the boundary between the inner rectangle (left) and the outer parts (right) of the annealed dendrite. The EBSD-patterns 1-8 were obtained at the locations 1-8; while the patterns 1, 2, and 5 show the same pattern originating from the BTS dendrite, the other patterns may all be indexed as the monoclinic high temperature phase with the composition $BaSi_2O_5$ previously detected in BTS glass ceramics grown via EiN but only in the immediate vicinity of the Pt-wire.[5] The primary BTS crystals now occupy more of the cut plane while the interdendritic spaces have shrunk and no longer contain the fine structures observed in Figure 5. Instead they contain well developed crystal bodies of BTS (same orientation as the primary structures, see EBSD-pattern 2) and µm scale crystals of $BaSi_2O_5$ as well as two phases highlighted by the white arrows which show differing SEM-contrasts and do not provide EBSD-patterns. Pores are also frequently observed and may be distinguished by the bright SEM-contrast caused by an edge effect, e.g. at the bottom of Figure 7 b).

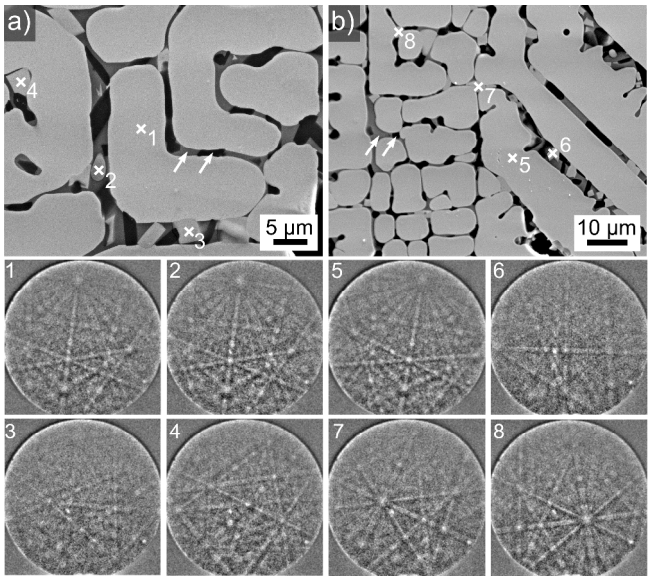

Figure 7: SEM-micrographs of a cut plane transecting an annealed BTS dendrite close to its origin a) at the core and b) at the boundary between the inner rectangle and the outer parts. The EBSD-patterns 1-8 were obtained at the locations 1-8.

Figure 8 presents comparable results from a) the core and b) the periphery of a cut plane of the same dendrite ca. 4 mm further from the Pt-wire. Figure 8 a) clearly shows that the fine structures observed in Figure 5 c) have coarsened while the superimposed orientation map of an EBSD-scan performed on the area proves that only minimal orientation deviations of less than 5° occur locally. The same was also observed in a number of scans performed on all cut planes prepared from this dendrite. While $BaSi_2O_5$ was not observed in the dendrite core in this cut plane, the phase map superimposed on Figure 8 b) illustrates that it frequently occurs in the interdendritic spaces of the outer parts of this cut plane. The area framed in Figure 8 a) provided a relatively large area containing the two remaining phases as illustrated below. The image quality (IQ)-map segment of the performed EBSD-scan does not show any difference between the darker and the brighter phase, indicating they are both very likely amorphous. The results of an EDX-mapping performed on the area are also presented and show that the darkest phase in the SEM-micrographs is mainly enriched in Si and O while the slightly brighter phase additionally contains

Al and K, both elements which are not supposed to be part of the initial glass composition. These impurities are most probably not contaminants from the furnace because they also occur in the bulk.

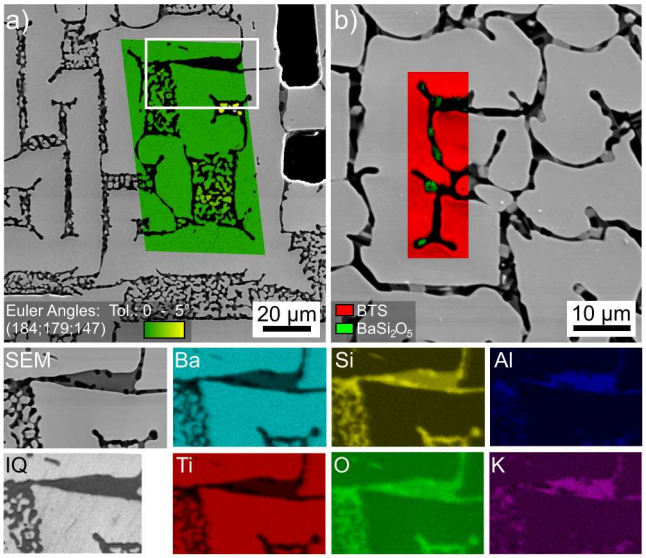

Figure 8: SEM-micrographs of a cut plane transecting the annealed BTS dendrite in Figure 7 ca. 4 mm from that cut plane a) at the core and b) in the outer parts. The micrographs are superimposed by a) the orientation map of an EBSD-scan and b) the phase map of an EBSD-scan. The SEM-micrograph as well as the IQ-map segment and EDX-mapping results of the framed area are presented below.

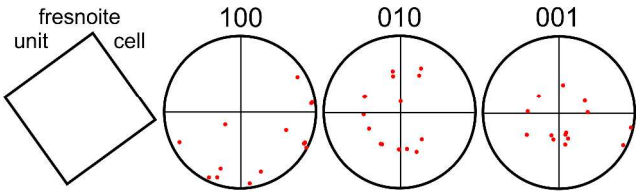

Figure 9: Unit cell illustrating the BTS dendrtite orientation as well as PFs of the main crystal directions of 17 $BaSi_2O_5$ individually analyzed crystals.

As $BaSi_2O_5$ only occurs in the form of small single crystals spaced fairly far apart in this material, a representative texture analysis is impractical. Instead, the 001, 010 and 001 poles of 17 individually analyzed $BaSi_2O_5$ crystals from various locations and cut planes of the same dendrite

were plotted into the pole figures (PFs) next to a wire frame in Figure 9 illustrating the BTS orientation. With only one exception, all the $BaSi_2O_5$ crystals show an orientation where the crystallographic a-axis is nearly perpendicular to the c-axis of the BTS dendrite. Due to this crystallographic relationship, it is likely that $BaSi_2O_5$ is preferably formed directly on the BTS lattice instead of forming independent nuclei in the residual glass. As the annealing temperature was significantly below the BTS melting temperature of 1445 °C and the crystal orientations of BTS in the interdendritic spaces basically remain constant, it may be concluded that a type of intragranular Ostwald Ripening occurred via diffusion at high temperatures. This is accompanied by an accumulation of impurities and residual melt components in the interdendritic spaces, leading to the crystallization of HT-$BaSi_2O_5$ and a phase separation of the remaining amorphous parts into one glass containing almost pure SiO_2 and a second glass containing SiO_2, BaO as well as the impurities Al and K. As the crystal orientation of the BTS component in this composite is practically not altered by this process, the high temperature applicability of these materials should not be affected.

The d_{33}-values of a 1 mm thick slab (8.0 x 13.2 mm^2) cut from the single crystal shown in Figure 1 a) were measured before and after annealing at 1150 °C for 21 h. The sputtered gold electrodes were chemically removed before annealing with a 1:3 mixture of HNO_3 and HCl. After annealing, the surfaces were repolished and contacted by new gold layers. The slab was cut and prepared so that the c-axis of the dendrite was approximately parallel to the measurement direction. Values of 3.7±0.3 and 4.0±0.2 x 10^{-12} m/V were respectively measured before and after annealing, indicating that the ripening process may actually increase the piezoelectric properties of these materials.

Values of 2.8 - 8.0 x 10^{-12} m/V are found in the literature for BTS single crystals[13,20-23] and values ranging from 2 to 13 x 10^{-12} m/V have been measured in BTS glass-ceramics produced via the surface crystallization of various glasses.[22-25] Here it must be noted that the values of 2 to 8 x 10^{-12} m/V were measured using d_{33}-meters[13,22,23] while values of 6.1 and 13 x 10^{-12} m/V were obtained using the Maker fringe technique.[24,25]

Dendrite Interaction during Growth

If the growing crystals are not drawn from the melt, neighboring BTS dendrites compete with each other as outlined in Figure 1 b). Figure 10 presents an SEM-micrograph of a cut plane transecting the dendrites featured in Figure 1 b). It is superimposed by the orientation maps of EBSD-scans performed on the surface which show that these dendrites systematically change their orientation as a function of the distance from the neighboring dendrite. In fact, the cross section shows three dendrites in the cut plane and a large pore near the contact area. The orientation maps in the right hand dendrite show that it systematically changes its orientation by 12° over a distance of ca. 1.5 mm, i.e. by 8°/mm. The left hand dendrite changes its orientation by ca. 2°/mm. These orientation changes are clearly more pronounced than the orientation changes observed in the dendrite presented in Figure 4 which grew without competition. Hence it is clear that stresses or varying melt conditions may lead to slight orientation changes during dendrite growth. These orientation changes are much smaller and have a different cause than those observed in the STS system where dendritic growth is observed at high temperatures but a different growth mechanism causing a fiber texture is observed at lower temperatures.[18] The inset in Figure 9 displays an orientation map superimposed on the pore showing the framed area in a higher magnification. It illustrates that some individual crystals deviate from the surrounding

orientation in agreement with the literature.[4,5] These crystals represent dendrite arms which have separated from the main body before cooling,[5] either by breaking or remelting,[19] and then shifting their position in the matrix.

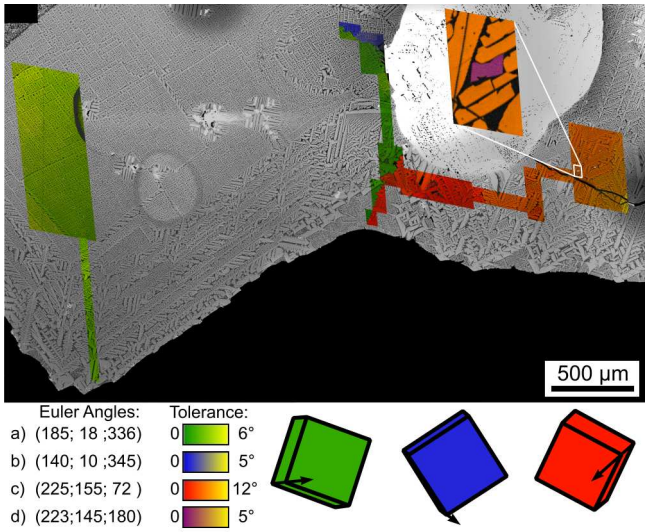

Figure 10: Systematic orientation deviation in two neighboring dendrites competing during growth.

Altogether four cut planes perpendicular to the average growth direction of these dendrites, not drawn from the melt, were analyzed to gain insight into the development of the irregular areas outside the central rectangle during growth. Figure 11 shows SEM-micrographs from the edge of the left hand dendrite in Figure 10. In cut plane 1 (near the growth front of the dendrite) the irregular part is very thin and continuously increases in thickness as the cut planes move towards the beginning of the dendrite, i.e. the Pt wire. It seems probable that the central rectangle is basically the area of the primarily formed dendrite, while the irregular areas form afterwards and allow an increase of the diameter after the primary growth front has passed.

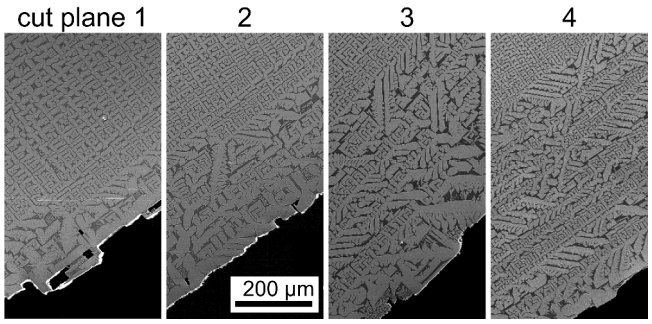

Figure 11: SEM-micrographs presenting the irregular area outside the central rectangle in four cut planes performed perpendicular to the growth direction from 1 the end of the dendrite to 4 closer to the beginning.

3. Experimental

The compounds $BaCO_3$, TiO_2 and SiO_2 (quartz) were mixed and subsequently melted in a platinum crucible (250 ml) at 1450 °C using an inductively heated furnace. The furnace was equipped with a lifting motor, which enabled to lift a platinum wire in and out of the melt. After 2 h soaking at 1500 °C, the platinum wire was inserted centrically into the melt. The melt was then cooled down to 1200 °C. During soaking for another 30 min, spontaneous crystallisation was not observed. To induce nucleation, an electric potential (4.8 V) between the Pt wire (cathode) and the crucible (anode) was applied, using a d.c. calibrator (Knick, Germany). This led to a current flow of 100 mA. As soon as crystallisation was observed after ca. 2 min, the Pt-wire was slowly drawn upward with 2-6 mm/min so that only the downward growing crystals remained in contact to the melt. Finally the platinum wire with the adjacent crystals was lifted out of the melt and cooled to room temperature with a cooling rate of 3 K/ min.

The samples were manually polished with shrinking grain sizes down to 0.75 µm diamond suspension. A final finish of 30 min. using colloidal silica was applied. Conductivity of the surface was achieved by mounting the sample using Ag-paste and applying a thin coating of carbon at about 10^{-3} Pa.

Optical micrographs were obtained using a Carl Zeiss Axio Imager Z1M LSM5-Pascal. Scanning electron microscopy (SEM) of uncoated samples was performed using a Jeol JSM-5610LV low-vacuum SEM at a pressure of 30 Pa. Most SEM analyses were performed using a Jeol JSM 7001F scanning electron microscope equipped with an EDAX Trident analyzing system containing a Digiview 3 EBSD-camera. EBSD-scans were performed using a voltage of 20 kV and a current of ca. 2.40 nA. The scans were captured and evaluated using the software TSL OIM Data Collection 5.31 and TSL OIM Analysis 6.2. Unreliable data points were removed in all datasets used for orientation analysis by applying a Confidence Index (CI) filter of 0.1 after performing a grain CI standardization. This results in only considering orientation solutions which are correct with a probability of at least 95 %.in EBSD-maps. No further cleanups which actually modify orientations were applied.

Piezoelectric measurements were performed using a d_{33}-meter (Sinocera YE2730A). Both sides of the sample were polished and contacted by sputtered gold electrodes of ca. 200 nm thickness (VEB Hochvakuum Dresden B30).

4. Conclusion

The performed experimental setup enables to produce macroscopic glass-permeated single-crystals of fresnoite. Multiple morphologies of the primary dendrites and the interdendritic area are observed after preparation. Annealing these materials at 1150 °C leads to the intergranular Ostwald Ripening of fresnoite where the degree of orientation remains practically unaffected. Small high temperature $BaSi_2O_5$ crystals with their a-axes predominantly oriented perpendicular to the c-axis of the BTS dendrite are also observed in the interdendritic spaces after annealing. Interactions between neighboring dendrites cause enhanced orientation changes.

5. Acknowledgments

This work was supported by Deutsche Forschungsgemeinschaft (DFG) in Bonn Bad Godesberg (Germany) via project nr. RU 417/14-1.

References

1. A. Keshavarzi, W. Wisniewski, C. Rüssel, *CrystEngComm* 2012, **14**, 6904–6909.
2. R. Keding, C. Rüssel, *Ber. Bunsenges. Phys. Chem.* 1996, **100**, 1515-1518.
3. T. Höche, R. Keding, C. Rüssel, *J. Mater. Sci.* 1999, **34**, 195-208.
4. W. Wisniewski, M. Nagel, G. Völksch, C. Rüssel, *Cryst. Growth Des.* 2010, **10**, 1939-1945.
5. W. Wisniewski, M. Nagel, G. Völksch, C. Rüssel, *Cryst. Growth Des.* 2010, **10**, 4526-4530.
6. M. Nagel, W. Wisniewski, G. Völksch, C. Borschel, C. Ronning, C. Rüssel, *CrystEngComm* 2011, **13**, 3383-3389.
7. R. Keding, C. Rüssel, *J. Mater. Sci.* 2004, **39**, 1433-1435.
8. R. Keding, C. Rüssel, *J. Non-Cryst. Solids* 2005, **351**, 1441-1446.
9. W. Wisniewski, R. Carl, C. Rüssel, *CrystEngComm* 2014, **16**,1192-1200.
10. R. Keding, D. Stachel, C. Rüssel, *J. Non-Cryst. Solids* 2001, **283**, 137-143.
11. O. Anspach, R. Keding, C. Rüssel, *J. Non-Cryst. Solids* 2005, **351**, 656-662.
12. K. Gerth, C. Rüssel, R. Keding, P. Schleevoigt, H. Dunken, *Phys. Chem. Glasses* 1999, **40**, 135-139.
13. A. Halliyal, A. S. Bhalla, S. A. Markgraf, L. E. Cross, R. E. Newnham *Ferroelectrics* 1985, **62**, 27–38.
14. J. Melngailis, J. F. Vetelino, A. Jhunjhunwala, T. B. Reed, R. E. Fahey, E. Stern, *Appl. Phys. Lett.* 1978, **32**, 203-205.
15. P. S. Bechthold, S. Haussühl, E. Michael, J. Eckstein, K. Recker, F. Wallrafen, *Phys. Lett.* 1978, **65A**, 453-454.
16. T. Höche, H.-J. Kleebe, R. Brydson. *Philos. Mag. A* 2001, **81**, 825-839.
17. L. Gránásy, T. Pusztai, T. Börzsönyi, J. A. Warren, J. F. Douglas, *Nature Mater.* 2004, **3**, 645-650.
18. W. Wisniewski, M. Patschger, C. Rüssel, *Sci. Rep. UK* 2013, **3**, 3558.
19. M. Rettenmayr, *In. Mater. Rev.* 2009*,* **54**, 1-17.
20. M. Kimura, K. Doi, S. Nanamatsu, T. Kawamura, *Appl. Phys. Lett.* 1976, **29**, 227-228.
21. M. Kimura, *J. Appl. Phys.* 1977, **48**, 2850-2856.
22. A. Halliyal, A. S. Bhalla, R. E. Newnham, L. E. Cross, *J. Mater. Sci.* 1981, **16**, 1023–1028.
23. A. Halliyal, A. Safari, A. S. Bhalla, R. E. Newnham, *Ferroelectrics* 1983, **50***,* 45–50.
24. Y. Takahashi, Y. Benino, T. Fujiwara, T. Komatsu, *J. Appl. Phys.* 2004, **95**, 3503-3508.
25. H. Masai, S. Tsuji, T. Fujiwara, Y. Benino, T. Komatsu, *J. Non-Cryst. Solids* 2007, **353**, 2258-2262.

Table of Contents Entry

Macroscopic Glass-Permeated Single-Crystals of Fresnoite

Wolfgang Wisniewski, Marcus Nagel, Christian Rüssel

Otto-Schott-Institut, Jena University, Fraunhoferstr. 6, 07743 Jena, Germany

Macroscopic single-crystals of fresnoite permeated by glass are grown by a Czochralski-like procedure for high temperature piezoelectric applications.